Photocatalytic Hydrogen Production Using Fe-Graphene/TiO2 Photocatalysts in the Presence of Polyalcohols as Sacrificial Agents

Naimah, Mu' to
Department of Chemical Engineering, Faculty of Engineering, Universitas Indonesia

Farashinta Dellarosa Nanda Pratama
Department of Chemical Engineering, Faculty of Engineering, Universitas Indonesia

Ibadurrohman, Muhammad
Department of Chemical Engineering, Faculty of Engineering, Universitas Indonesia

https://doi.org/10.5109/6625736

出版情報：Evergreen. 9 (4), pp.1244-1251, 2022-12. 九州大学グリーンテクノロジー研究教育センター
バージョン：

Photocatalytic Hydrogen Production Using Fe-Graphene/TiO_2 Photocatalysts in the Presence of Polyalcohols as Sacrificial Agents

Mu'to Naimah[1], Farashinta Dellarosa Nanda Pratama[1], Muhammad Ibadurrohman[1,*]

[1]Department of Chemical Engineering, Faculty of Engineering, Universitas Indonesia, Indonesia

*Author to whom correspondence should be addressed:
E-mail: ibad@che.ui.ac.id

(Received February 11, 2022; Revised December 16, 2022; accepted December 25, 2022).

Abstract: Modifications of TiO_2 in photocatalytic hydrogen production have been widely studied to resolve its limitations in harnessing visible light and electron-hole recombination. Among them is by the combination of Graphene and Fe dopant. This study examines the effects of various concentrations of Fe on Fe-Graphene/TiO_2 and various polyalcohols as sacrificial agents for H_2 production. Graphene/TiO_2 and Fe-Graphene/TiO_2 were synthesized by a wet-impregnation method. Characterizations were applied on TiO_2 P25, Graphene/TiO_2, and Fe-Graphene/TiO_2, using XRD, SEM-EDX, UV-Vis DRS, and FTIR techniques to analyze the properties of the catalysts. H_2 production experiment was carried out for 5 h in a reactor that enables internal illumination, equipped with a 20W UV lamp, burette, and cooling water. GC analysis of gas sample on the burette confirmed the formation of hydrogen. The accumulation of H_2 products indicated that 0.2% Fe on Fe-Graphene/TiO_2 with a bandgap of 3.03 eV offers up to 80% higher H_2 production than TiO_2 P25. Photocatalytic H_2 production with Fe-Graphene/TiO_2 and 10% v/v alcohols as sacrificial agents were revealed to decrease in the following order: glycerol > ethylene glycol > methanol > propylene glycol > n-propanol. Correlations were obtained between H_2 yield and key alcohol properties, notably the number of α-H, polarity, and oxidation potential of the alcohols.

Keywords: Fe-Graphene/TiO_2; Hydrogen; Photocatalytic; Polyalcohol; Sacrificial Agent

1. Introduction

Energy plays an important role in supporting a majority of demands on various sectors, ranging from industrial, transportation, to household needs. However, energy consumption both in Indonesia and worldwide is still centered on fossil fuel energy sources, including gas, oil, and coal[1),2)]. Fossil-based fuels produce CO_2 emissions that can cause negative impacts on the environment, especially global warming events. Therefore, hydrogen as an alternative energy source can be a solution in replacing fossil fuels. Conventional technologies in producing hydrogen, such as steam reforming, partial oxidation, or water gas shift, have limitations on the high energy requirements[3)]. An alternative to circumvent this issue is through a route of hydrogen production that is more economical and environmentally friendly, namely the photocatalytic water splitting using solar as an energy source. Photocatalysis is a versatile technology that offers alternative routes for many processing applications[4-8)].

Photocatalytic water splitting is a heterogeneous process that takes place under photon illumination and requires semiconductor materials. In a water-splitting process, titanium dioxide or titania (TiO_2) is generally used as a photocatalyst for various purposes[9)]. TiO_2 semiconductor is widely used because its bandgap (E_g) straddles the redox potentials of oxygen and hydrogen. However, for the same reason, the bandgap of TiO_2 is ca. 3.2 eV, implying that TiO_2 can only utilize UV spectra, which accounts for only 3% in the solar light[10)]. Furthermore, the recombination of excitons (electron-hole pairs) has also been revealed to be the bottleneck for the efficient process of titania-based photo-splitting. To resolve these limitations, many studies have been conducted by pursuing various modifications of TiO_2[11-13)]. One of them is through the combination of Graphene and Fe as promotors, which have been reported to increase the photocatalytic activity of TiO_2. Isari et al.[14)] reported that the use of Fe-TiO_2/rGO photocatalyst can reduce the bandgap down to 2.76 eV.

Fe ions can be easily doped on TiO_2 crystal lattice because their atomic size is close to Ti atom[15)]. Graphene in photocatalytic applications can increase semiconductors activity due to its high carrier mobility and large surface area[16)]. Research by Shende et al.[17)] showed that Graphene-Fe-TiO_2 photocatalyst could drive

the crystal violet dye degradation of up to 74.6%, higher than the use of Graphene-Ce-TiO_2 which reach only 58.7%. In another report, even in the case where no sacrificial agent is present, Fe/TiO_2/rGO was able to produce hydrogen up to 10 μmol/g in 5 h[16]. Despite its vast potentials, however, research reports regarding Fe-Graphene/TiO_2 as photocatalysts for hydrogen production are still limited, hence further development is needed. In this paper, we report Fe-Graphene/TiO_2 for photocatalytic hydrogen production, examining the effects of concentrations of Fe doping and various polyalcohols as sacrificial agents.

2. Experimental Methods

2.1 Synthesis of Photocatalysts

Graphene/TiO_2 was synthesized by a wet-impregnation method. An amount of 5 mg of Single-Layer Graphene (ACS Material) was firstly dissolved in 100 ml ethanol/water (volume ratio of 4:1) solution using an ultrasonic bath for 1 h. An amount of 1 g of TiO_2 P25 (Evonik) was then introduced into the solution and vigorously stirred for 1 h, followed by 1 h of sonication. The attained suspension was centrifuged several times for 1 h before it was dried in an oven for 2 h at 80°C. The resultant Graphene/TiO_2 precipitate was ground and, subsequently, the powder was calcined at 400°C for 2 h.

Preparation of Fe-Graphene/TiO_2 was carried out using the same wet-impregnation method. Initially, 5 mg of Single-Layer Graphene (ACS Material) was dispersed in 45 ml absolute ethanol for 45 mins. An amount of 1 g of TiO_2 P25 (Evonik) was then introduced into the solution and dispersed using an ultrasonic instrument for another 45 mins. The solution on the beaker was stirred until homogeneity is achieved using a magnetic stirrer for 2 h. Subsequently, a solution containing 14.5; 36.2; 50.7 mg (0.2; 0.5; 0.7% Fe, respectively) of $Fe(NO_3)_3.9H_2O$ (Merck) as a precursor of iron and 10 ml absolute ethanol was added drop wisely into the mixture under vigorous stirring, and the stirring continued overnight. The attained gel was dried for 2 h in an oven at 80°C, then grounded using mortar and pestle. Finally, the resulted powder of Fe-Graphene/TiO_2 was calcined at 400°C for 2 h.

2.2 Material Characterization

Photocatalyst characterization was done on TiO_2 P25, Graphene/TiO_2, and Fe-Graphene/TiO_2 with a Fe doping concentration of 0.2%. The crystal phase of the photocatalysts was checked by X-ray diffraction (XRD, PANalytical Aeris), which scanning range was 2θ = 5-90°. A scanning electron microscope (SEM, FEI Quanta 650 FEG) was used to detect the morphology and structure of the catalysts, while the composition of atomic elements on the surface of the photocatalyst was identified with energy dispersive X-ray (EDX, Oxford Instruments Xplore 15). Optical absorption properties of the photocatalyst samples over the range of 200 nm to 800 nm were recorded using UV-Vis diffuse reflectance spectra (DRS, Agilent Cary 60 UV-Vis). To verify the several functional groups present in the prepared photocatalysts, Fourier-transform infrared (FTIR, Thermo Scientific Nicolet iS5) was utilized in the range of 4000-400 cm^{-1}.

2.3 Photocatalytic Hydrogen Production Test

The photocatalytic hydrogen production tests were conducted in a reactor with a configuration that enables internal illumination. For each measurement, 0.2 g photocatalyst is added to 320 ml alcohol-water mixtures, containing 10% v/v alcohol. A range of alcohols are utilized as sacrificial agents, namely: methanol (CH_4O), n-propanol (C_3H_8O), ethylene glycol ($C_2H_6O_2$), propylene glycol ($C_3H_8O_2$), glycerol ($C_3H_8O_3$). Continuous stirring is applied throughout the reaction, and the headspace of the reactor was connected to an inverted burette filled with water at atmospheric pressure to measure the evolved hydrogen volume. The reactor was also equipped with a cooling water system maintained at 25°C to compensate for the generated heat from photon exposure, and a thermometer to monitor the temperature of the reactor. Before light illumination, purging with argon flow followed by leakage testing was done for 15 mins each to remove air on the reactor and to ensure no leak during the tests. The reaction was performed for 5 h with a 20 W UV lamp as the light source. Sampling was done by recording the amount of gas evolved in the burette periodically. The hydrogen gas product accumulated on top of the burette was characterized by gas chromatography (GC, Shimadzu GC-8A) to confirm the formation of hydrogen. Total hydrogen volumes data obtained were calculated to moles by assuming that the gas behaves as an ideal gas.

3. Results and Discussion

3.1 Photocatalyst Characterization

3.1.1 XRD Analysis

The characteristic diffraction peaks of anatase and rutile phases ascribed to TiO_2 are shown in Figure 1 (a). The anatase phase was identified by peaks that appear at 2θ = 25.2°, 37.7°, 47.8°, 53.8°, 54.9°, 62.5°, 68.6°, 70.1°, and 74.8°, which represent the indices of (1 0 1), (0 0 4), (2 0 0), (1 0 5), (2 1 1), (2 0 4), (1 1 6), (2 2 0), and (2 1 5) facets, respectively. Meanwhile, a minor part of the rutile phase was detected by 2θ peaks at 27.5° and 36.1°, indexed to (1 1 0) and (1 0 1) facets. No other diffraction peaks are observed as a result of Graphene addition because Graphene is typically amorphous or not having a fixed crystal structure[18]. The XRD profile of Fe-Graphene/TiO_2 on (1 0 1) plane displays a slight, yet observable, shift of diffraction signal to a higher 2θ value (Figure 1 (b)). This may indicate that some Fe(III) cations might be substituted into TiO_2 lattice due to the smaller ionic radius of Fe^{3+} (0.64 Å) compared to Ti^{4+} (0.68 Å)[19]. The crystallite size of the photocatalysts estimated using the Scherrer equation shows a decreasing crystallite size

(Table 1). This can be caused by Graphene and Fe as additives that suppress the crystal growth of TiO_2, hence inhibiting contact between TiO_2 particles for sintering to take place[14),20)].

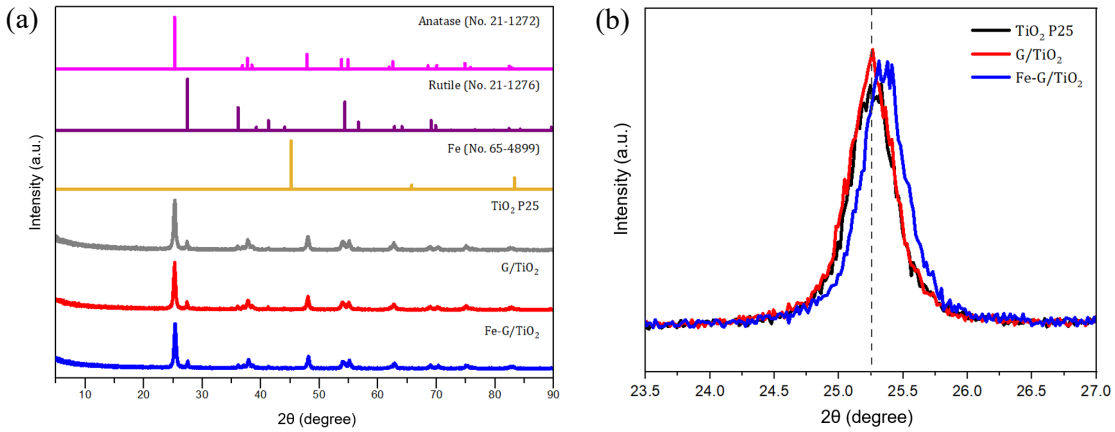

Fig. 1: (a) XRD patterns of TiO_2 P25, G/TiO_2, and Fe-G/TiO_2 (b) XRD magnification on (1 0 1) plane

Table 1. Photocatalyst crystallite size

Photocatalyst	2θ	FWHM	Crystallite Size (nm)
TiO_2 P25	25.260	0.460	17.681
G/TiO_2	25.253	0.461	17.661
Fe-G/TiO_2	25.347	0.537	15.163

3.1.2 SEM-EDX Analysis

Figure 2 shows the surface morphology of the prepared photocatalysts. As depicted in the figure, both Graphene/TiO_2 and Fe-Graphene/TiO_2 display a typical morphology that consists of domains of aggregated particles. No specific characteristic differences were identified between photocatalysts surface morphology due to the small magnification and much higher content of TiO_2. From Table 2, it can be seen that all photocatalysts are characterized to show the existence of Ti and O elements. Fe dopant presence on Fe-Graphene/TiO_2 was also detected in the EDX results. However, it is at a different loading content (0.4%) from the theoretical one (0.2%). This happened because of the relatively small concentration of Fe dopant, which made it difficult to precisely control the amount of $Fe(NO_3)_3.9H_2O$ as a precursor due to its hydrates presence.

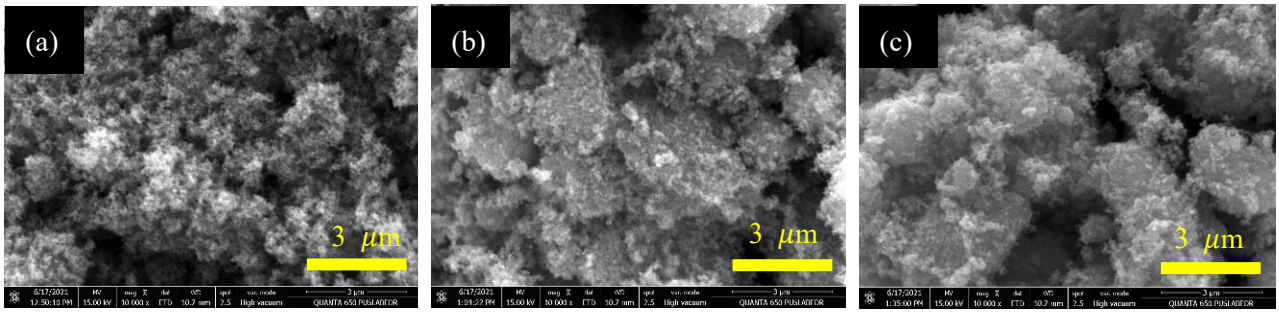

Fig. 2: Surface morphology of (a) TiO_2 P25, (b) G/TiO_2, and (c) Fe-G/TiO_2, with 10.000x magnification

Table 2. Photocatalyst EDX result

Photocatalyst	Theoretical Content (wt%)		Actual Content (wt%)		
	Graphene	Fe	Ti	O	Fe
TiO_2 P25	-	-	56.46	43.54	-
G/TiO_2	0.50	-	59.13	40.87	-
Fe-G/TiO_2	0.50	0.20	54.59	45.01	0.40

3.1.3 UV-Vis DRS Analysis

The resultant UV-Vis spectra (Figure 3) reveal slight variations in absorption intensity of TiO_2 P25, Graphene/TiO_2, and Fe-Graphene/TiO_2. Within the range

of 400-800 nm, TiO_2 P25 appears to exhibit weaker absorbance as compared to its photocatalyst counterparts. In the visible light region, Graphene/TiO_2 has slightly better absorption intensity than TiO_2 P25, suggesting a moderate role of Graphene as a photosensitizer. Moreover, Fe doping on Fe-Graphene/TiO_2 shows greater absorbance responses than Graphene/TiO_2. Near the conduction band of TiO_2, Fe ions can form an impurity energy level, thus allowing electrons to be excited from the valence band to the intermediate level by absorbing light in the visible region[16].

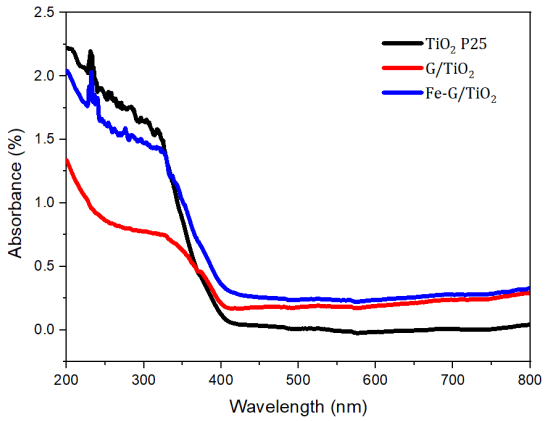

Fig. 3: UV-Vis spectrum comparison of TiO_2 P25, G/TiO_2, and Fe-G/TiO_2

Bandgap energy can be calculated using Tauc Plot between $(F(R)hv)^{1/2}$ vs photon energy (hv). The bandgap of all photocatalysts is tabulated in Table 3. It implies that Fe-Graphene/TiO_2 has the lowest bandgap as compared to TiO_2 P25 and Graphene/TiO_2. This inferred the notable effects of Graphene and Fe combination on the optical characteristics of the photocatalyst, which has been documented to be able to promote band gap lowering through the formation of intermediate energy band near TiO_2 conduction band[21].

Table 3. Bandgap energy

Photocatalyst	Bandgap (eV)
TiO_2 P25	3.14
G/TiO_2	3.08
Fe-G/TiO_2	3.03

3.1.4 FTIR Analysis

The results of FTIR characterization in Figure 4 show absorption peaks of the photocatalysts at wavenumbers of 4000-400 cm^{-1}. Absorption peaks in the wavenumber region of 590 cm^{-1} and 1403 cm^{-1} of all photocatalysts indicate stretching vibrations of Ti-O and Ti-O-Ti bond. The appearance of a specific absorption peak that distinguishes Fe-Graphene/TiO_2 from TiO_2 P25 and Graphene/TiO_2 occurs at 1326.46 cm^{-1}. Epoxidation of C-O-C functional group is generally identified in this range (1280-1320 cm^{-1}), indicating an influence of Graphene[22]. The presence of Graphene on Graphene/TiO_2 can also be identified by Ti-O-C vibrations at 3230 cm^{-1}. Absorption of Fe-Graphene/TiO_2 at wavenumber of 1634 cm^{-1} was greater than TiO_2 P25 (1633.70 cm^{-1}) and Graphene/TiO_2 (1631.03 cm^{-1}). This absorption peak corresponds to a surface hydroxylation due to the existence of Fe dopant on TiO_2[23]. The addition of Fe dopant causes fewer electrons at $3d^6 4s^2$ level to absorb photons, resulting in an increase in transmission which is identified by a specific absorption peak shift[24].

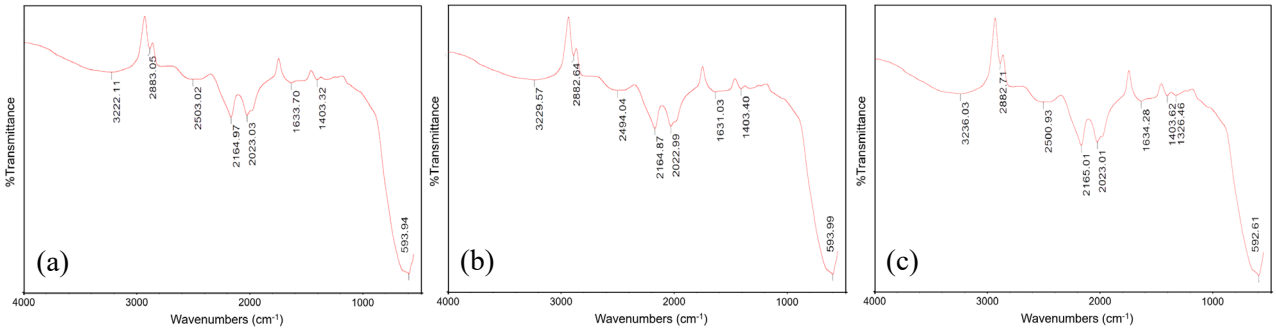

Fig. 4: IR spectra of (a) TiO_2 P25, (b) G/TiO_2, and (c) Fe-G/TiO_2

3.2 Photocatalytic Activity for H_2 Production

3.2.1 Effect of Fe Concentration

At optimum concentration, Fe is a promising cocatalyst because it can increase the number of active sites on the catalysts, reduce the bandgap of TiO_2, and decrease the electron-hole recombination rate[25]. As inferred from Figure 5, 0.2%Fe-Graphene/TiO_2 offers the highest amount of hydrogen produced (394.2 µmol) relative to its photocatalyst counterparts. On the other hand, 0.5%Fe-Graphene/TiO_2, which was expected to be the optimum Fe loading in a Fe-Graphene-TiO_2 system according to Khalid et al.[26], produced only 314.6 µmol of hydrogen. This can be explained by the differences in experiments system configuration and characteristics of the Graphene used. Further addition of Fe into the composite is detrimental to the amount of hydrogen produced, such as in the case of 0.7%Fe-Graphene/TiO_2 (171.4 µmol). In the case where Fe^{3+} doping is too high, the distance between the traps (hole scavenger) can substantially decrease, turning Fe sites into recombination centers[27]. Moreover,

the addition of Fe above the optimum concentration also results in excessive Fe ions that hinder interaction between TiO_2 and the incoming photons. Excess of Fe may also lead to poor incorporation on TiO_2 crystal lattice, which in turn reduce photocatalyst crystallinity, thus compromising the photocatalytic capacity[28].

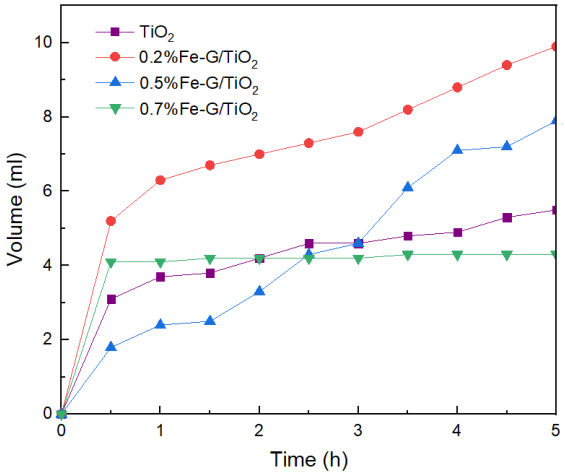

Fig. 5: Hydrogen production with Fe-G/TiO_2 and 10% v/v glycerol at various Fe concentrations

Table 4. Hydrogen production comparison

Photocatalyst	H_2 Produced (µmol)
TiO_2 P25	219.3
0.2%Fe-G/TiO_2	394.2

As shown in Table 4, 0.2%Fe-Graphene/TiO_2 gives hydrogen production up to 80% higher than TiO_2 P25. It suggests at this concentration, it is an optimum Fe loading that is not too high to cause recombination center formation, shielding effect, or reduced crystallinity, as mentioned above. With more hydrogen production by Fe-Graphene/TiO_2 catalyst, it also signifies the role of Graphene and Fe as a transition metal dopant that function effectively as electron trappers in inhibiting electron-hole recombination.

3.2.2 Effect of Polyalcohol Sacrificial Agent

Hydrogen accumulation from different sacrificial agent solutions appear to decrease in the following order: glycerol > ethylene glycol > methanol > propylene glycol > n-propanol, as depicted in Figure 6. The highest hydrogen production of 394.2 µmol was obtained with glycerol solution, confirming glycerol as a sacrificial agent that acts effectively as an electron donor on the anodic part of the redox reaction wherein it reacts with holes and/or hydroxyl radicals formed on TiO_2 surface[29]. Through the experiment with Fe-Graphene/TiO_2, it was also revealed that glycerol and ethylene glycol (394.2 µmol and 342.6 µmol, respectively) have superior hydrogen production compared to the other alcohols. Meanwhile, propylene glycol which is also classified as glycol (2 -OH) like ethylene glycol, appears to offer lower hydrogen production. This denotes that hydrogen production is related to other factors that can affect alcohol performance as a sacrificial agent. The production of H_2 can be examined based on the structure and physical properties of the alcohols used, as in Table 5 which summarizes key characteristics of the alcohols, and Figure 7 which shows a plot of hydrogen production against physical properties of the alcohols.

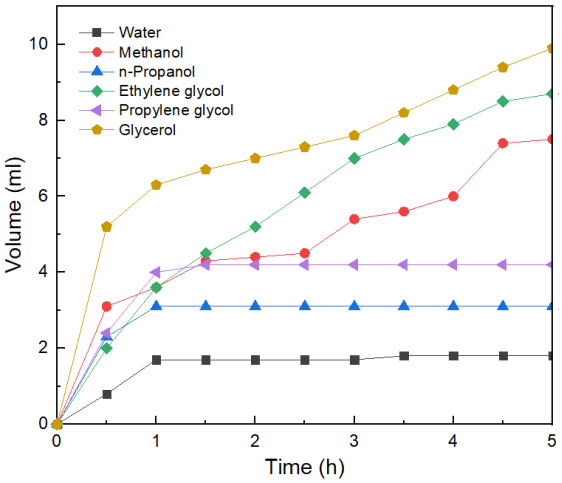

Fig. 6: Hydrogen production with 0.2%Fe-G/TiO_2 and various 10% v/v sacrificial agents

The photoreforming reaction of alcohols is generally written as follows[31]:

$$C_pH_qO_r + (2p - r)H_2O \rightarrow pCO_2 + xH^+ + xe^- \quad (1)$$

where p, q, and r, are the number of carbon, hydrogen, and oxygen atoms in the alcohol, respectively, while x is the number of protons or electrons discharged. Photoreaction in aqueous media occurs through the formation of alpha hydroxyl radicals, which can be detected on TiO_2 by Electronic Paramagnetic Resonance (EPR) technique[31].

$$RCH_2 - OH(a) + h^+(VB) \rightarrow RCH \cdot -OH(a) + H^+ \quad (2)$$

$$R_2CH - OH(a) + h^+(VB) \rightarrow R_2C \cdot -OH(a) + H^+ \quad (3)$$

This reaction mechanism highlights the importance of α-H in the chemical structure of an alcohol sacrificial agent to obtain high hydrogen production. n-Propanol which has the lowest number of α-H compared to the other alcohols was also seen to have the lowest hydrogen accumulation of only 123.8 µmol (Table 5).

The plot of hydrogen production to the number of OH groups and α-H atoms of alcohols shows a relationship between the two variables, as depicted in Figure 7 (a) and (b), respectively. The number of hydroxyl groups can affect the ease of alcohol photoreforming[29], with alcohols having C:O ratio = 1 (methanol, ethylene glycol, glycerol), easier to completely oxidize than alcohol with C:O ratio = 3 (n-propanol). In addition, alcohols with high polarity will interact strongly with the TiO_2 surface, allowing in more electrons being injected into the valence band of TiO_2[30]. The standard oxidation potential of each alcohol can also be considered. Standard oxidation potential (E^o_{ox}) vs NHE of alcohols which are lower than water (1.23 V vs NHE) denotes that the alcohols are more preferred as oxidation targets in the alcohol-water system[31].

Table 5. The characteristics of alcohols used in the H_2 production experiment with Fe-G/TiO_2

Sacrificial Agent	Number of OH	Number of α-H	C:O Ratio	Polarity[30]	E^o_{ox} (V) vs NHE[30]	H_2 Produced (μmol)
Water	1	0	0	0.963	1.230	72.0
Methanol	1	3	1	0.914	0.016	297.8
n-Propanol	1	2	3	0.864	0.100	123.8
Ethylene glycol	2	4	1	0.924	0.009	342.6
Propylene glycol	2	3	1.5	0.912	0.047	166.6
Glycerol	3	5	1	0.939	0.004	394.2

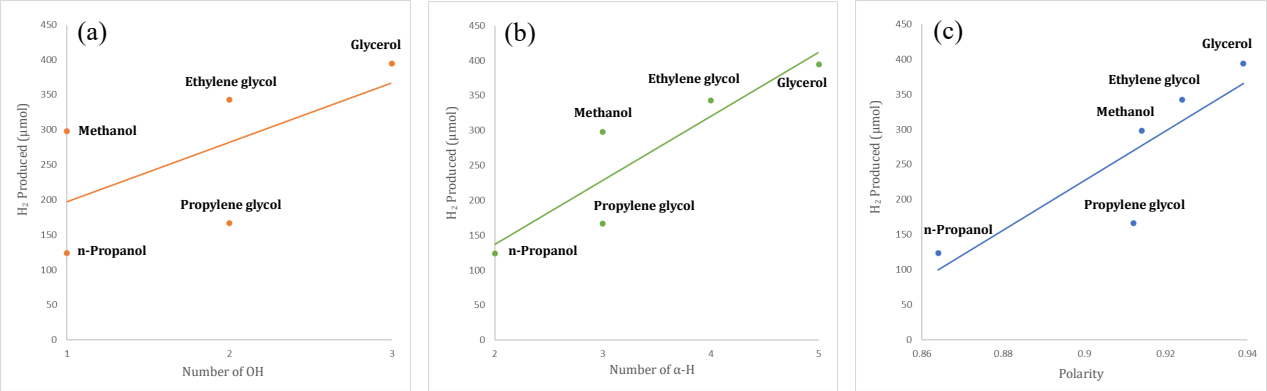

Fig. 7: The plot of hydrogen production with various 10% v/v sacrificial agents versus (a) Number of OH groups, (b) Number of α-H, and (c) Alcohol polarity

According to Chen et al.[31], the greater the distance between the valence band potential of TiO_2 (2.7 V vs NHE for anatase) to the oxidation potential of alcohols as donor, the higher the amount of hydrogen produced. Experimental results in this study agree with these statements, where the amount of hydrogen accumulated decreases in the order: glycerol > ethylene glycol (1,2-ethanediol) > methanol > propylene glycol (1,2-propanediol) > n-propanol. Furthermore, photocatalytic activity against propylene glycol displays slight variations from that reported by Al-Azri et al.[30]. In their work, the hydrogen produced with propylene glycol (21.9 mmol/g.h) was close to that of ethylene glycol (20.6 mmol/g.h). This difference can be explained because more complex alcohols are likely to form a number of other intermediates that can interfere with the formation of hydrogen[32]. Another possible reason is the possible presence of oxidation reaction products that poison photocatalyst surface[31].

4. Conclusion

Based on the results of the study, it can be concluded that the combination of Graphene and Fe dopant on Fe-Graphene/TiO_2 with optimum Fe concentration of 0.2% increases hydrogen production for up to 80% higher than TiO_2 P25, with a total of hydrogen produced were 394.2 μmol and 219.3 μmol, respectively. The correlation was obtained between alcohol properties, notably the number of α-H, polarity, and oxidation potential of the alcohols, to the amount of hydrogen produced. Hydrogen production with various 10% v/v sacrificial agents was revealed to decrease in the following order: glycerol > ethylene glycol > methanol > propylene glycol > n-propanol, with the hydrogen accumulated were 394.2 μmol, 342.6 μmol, 297.8 μmol, 166.6 μmol, and 123.8 μmol, respectively.

Acknowledgements

This research was financially supported by the Directorate of Research and Community Engagement Universitas Indonesia (DRPM UI) through International Indexed Publication Grant (PUTI Saintekes 2020) with Contract Number:NKB-4977/UN2.RST/HKP.05.00/2020.

References

1) V. Smil, "Energy Transitions: Global and National Perspectives," ABC-CLIO, 2017. https://books.google.co.id/books/about/Energy_Transitions.html?id=loKnDAEACAAJ&redir_esc=y.
2) "Indonesia Energy Outlook," 2019. https://www.esdm.go.id/assets/media/content/content-outlook-energi-indonesia-2019-bahasa-indonesia.pdf (accessed July 1, 2021).
3) N. Luo, Z. Jiang, H. Shi, F. Cao, T. Xiao, and P. Edwards, "Photo-catalytic conversion of oxygenated hydrocarbons to hydrogen over heteroatom-doped TiO_2 catalysts," *Int. J. Hydrog. Energy*, **34** (*1*) 125–129 (2009). doi:10.1016/j.ijhydene.2008.09.097.
4) M.T. Adiwibowo, M. Ibadurrohman, and Slamet, "Synthesis of ZnO Nanoparticles and their Nanofluid

Stability in the Presence of a Palm Oil-based Primary Alkyl Sulphate Surfactant for Detergent Application," *Int. J. Technol.*, **9** (*2*) 307–316 (2018). doi:10.14716/ijtech.v9i2.1065.

5) G.D. Junior, M. Ibadurrohman, and Slamet, "Synthesis of eco-friendly liquid detergent from waste cooking oil and ZnO nanoparticles," *AIP Conf. Proc.*, **2085** (*1*) 020075 (2019). doi:10.1063/1.5095053.
6) Slamet, M. Ibadurrohman, and P.P. Wulandari, "Synthesis of methyl ester sulfonate surfactant from crude palm oil as an active substance of laundry liquid detergent," *AIP Conf. Proc.*, **1904** (*1*) 020058 (2017). doi:10.1063/1.5011915.
7) I.H. Dwirekso, M. Ibadurrohman, and Slamet, "Synthesis of TiO_2-SiO_2-CuO Nanocomposite Material and Its Activities for Self-cleaning," *Evergreen*, **7** (*2*) 285–291 (2020). doi:10.5109/4055234.
8) N.I.I. Zamri, S.L.N. Zulmajdi, E. Kusrini, K. Ayuningtyas, H.M. Yasin, and A. Usman, "Rhodamine B Photocatalytic Degradation using CuO Particles under UV Light Irradiation for Applications in Industrial and Medical Fields," *Evergreen*, **7** (*2*) 280–284 (2020). doi:10.5109/4055233.
9) A.L. Linsebigler, L. Guangquan, and J. Yates, "Photocatalysis on TiO_2 Surfaces: Principles, Mechanisms, and Selected Results," *Chem. Rev.*, **95** (*3*) 735–758 (1995). doi:10.1021/cr00035a013.
10) M. Ni, M.K.H. Leung, D.Y.C. Leung, and K. Sumathy, "A review and recent developments in photocatalytic water-splitting using TiO_2 for hydrogen production," *Renew. Sustain. Energy Rev.*, **11** (3) 401–425 (2007). doi:10.1016/j.rser.2005.01.009.
11) M. Ezaki, and K. Kusakabe, "Highly crystallized tungsten trioxide loaded titania composites prepared by using ionic liquids and their photocatalytic behaviors," *Evergreen*, **1** (*2*) 18–24 (2014). doi:10.5109/1495159.
12) K. Taira, and H. Einaga, "Distribution ratio of Pt on anatase and rutile TiO_2 Particles, determined by x-ray diffraction and transmission electron microscopy analysis of Pt/TiO_2(P25)," *Evergreen*, **5** (*4*) 13–17 (2018). doi:10.5109/2174853.
13) A. Azani, D.S.C. Halin, M.M.A.B. Abdullah, K.A. Razak, M.F.S.A. Razak, M.M.D. Ramli, M.A.A.M. Salleh, and V. Chobpattana, "The effect of GO/TiO_2 thin film during photodegradation of methylene blue dye," *Evergreen*, **8** (*3*) 556–564 (2021). doi:10.5109/4491643.
14) A.A. Isari, A. Payan, M. Fattahi, S. Jorfi, and B. Kakavandi, "Photocatalytic degradation of rhodamine B and real textile wastewater using Fe-doped TiO_2 anchored on reduced graphene oxide (Fe-TiO/rGO): Characterization and feasibility, mechanism and pathway studies," *Appl. Sci.*, **462** 549–564 (2018). doi:10.1016/j.apsusc.2018.08.133.
15) R.D.S. Santos, G.A. Faria, C. Giles, C.A.P. Leite, H.D.S. Barbosa, M.A.Z. Arruda, and C. Longo, "Iron insertion and hematite segregation on Fe-doped TiO_2 nanoparticles obtained from sol-gel and hydrothermal methods," *ACS Appl. Mater. Interfaces*, **4** (10) 5555–5561 (2012). doi:10.1021/am301444k.
16) W. Feng, and J. Wu, "Photocatalytic reduction of CO_2 under visible light over Fe/TiO_2/rGO Nanocomposites by one-step Hydrothermal Synthesis," *IOP Conf. Ser.: Earth Environ. Sci.*, **513** 012012 (2020). doi:10.1088/1755-1315/513/1/012012.
17) T.P. Shende, B.A. Bhanvase, A.P. Rathod, D.V. Pinjari, and S.H. Sonawane, "Sonochemical synthesis of Graphene-Ce-TiO_2 and Graphene-Fe-TiO_2 ternary hybrid photocatalyst nanocomposite and its application in degradation of crystal violet dye," *Ultrason. Sonochem.*, **41** 582–589 (2018). doi:10.1016/j.ultsonch.2017.10.024.
18) H.F. Makki, and H.H. Alwan, "Synthesis and characterization of Graphene produced from Iraqi date syrup," *J. Eng. Sci.*, **26** (*1*) 49–54 (2019). doi:10.33261/jaaru.2019.26.1.007.
19) R. Faurani, A. Aritonang, and Harlia, "Sintesis dan Karakterisasi TiO_2/Ti Terdoping Fe(III) menggunakan Metode Anodisasi In-Situ," *Jurnal Kimia Khatulistiwa*, **8** (*2*) 73 – 81 (2019).
20) J. Yu, J.C. Yu, and X. Zhao, "The effect of SiO_2 addition on the grain size and photocatalytic activity of TiO_2 thin films," *J. Sci. Technol.*, **24** (*2*) 95–103 (2002). doi:10.1023/A:1015258105966.
21) L. Wasu, and B. Virote, "Enhancing the photocatalytic activity of TiO_2 co-doping of Graphene–Fe^{3+} ions for formaldehyde removal," *J. Environ. Manage.*, **127** 142–149 (2013). doi:10.1016/j.jenvman.2013.04.029.
22) P. Steiner, "Nanoscopic infrared characterisation of Graphene oxide," *thesis*, The University of Manchester (2018).
23) T. Ali, P. Tripathi, A. Azam, W. Raza, A.S. Ahmed, A. Ahmed, and M. Muneer, "Photocatalytic performance of Fe-doped TiO_2 nanoparticles under visible-light irradiation," *Mater. Res. Express*, **4** (*1*) 015022 (2017). doi:10.1088/2053-1591/aa576d.
24) M.B. Marami, M. Farahmandjou, and B. Khoshnevisan, "Sol-Gel Synthesis of Fe-Doped TiO_2 Nanocrystals," *J. Electron. Mater.*, **47** (*7*) 3741–3748 (2018). doi:10.1007/s11664-018-6234-5.
25) S. Sun, J. Ding, J. Bao, C. Gao, Z. Qi, X. Yang, B. He, and C. Li, "Photocatalytic degradation of gaseous toluene on Fe-TiO_2 under visible light irradiation: A study on the structure, activity and deactivation mechanism," *Appl. Surf. Sci.*, **258** (*12*) 5031–5037 (2012). doi:10.1016/j.apsusc.2012.01.075.
26) N.R. Khalid, Z. Hong, E. Ahmed, Y. Zhang, H. Chan, and M. Ahmad, "Synergistic effects of Fe and Graphene on photocatalytic activity enhancement of TiO_2 under visible light," *Appl. Surface Sci.*, **258** (*15*) 5827–5834 (2012). doi:10.1016/j.apsusc.2012.02.110.
27) J. Shi, G. Chen, G. Zeng, A. Chen, K. He, Z. Huang,

L. Hu, J. Zeng, J. Wu, and W. Liu, "Hydrothermal synthesis of graphene wrapped Fe-doped TiO_2 nanospheres with high photocatalysis performance," *Ceram. Inter.*, **44** (*7*) 7473–7480 (2018). doi:10.1016/j.ceramint.2018.01.124.

28) N. Farhangi, S. Ayissi, and P.A. Charpentier, "Fe doped TiO_2–Graphene nanostructures: synthesis, DFT modeling and photocatalysis," *Nanothechnology*, **25** (*30*) 305601–305611 (2014). doi:10.1088/0957-4484/25/30/305601.
29) W-T. Chen, Y. Dong, P. Yadav, R.D. Aughterson, D. Sun-Waterhouse, and G.I.N. Waterhouse, "Effect of alcohol sacrificial agent on the performance of Cu/TiO_2 photocatalysts for UV-driven hydrogen production," *Appl. Catal. A: Gen.*, **602** 117703 (2020). doi:10.1016/j.apcata.2020.117703.
30) Z.H.N. Al-Azri, W-T. Chen, A. Chan, and V. Jovic, "The roles of metal co-catalysts and reaction media in photocatalytic hydrogen production: Performance evaluation of M/TiO_2 photocatalysts (M = Pd, Pt, Au) in different alcohol–water mixtures," *J. Cat.*, **329** 355–367 (2015). doi:10.1016/j.jcat.2015.06.005.
31) W-T. Chen, A. Chan, Z.H.N. Al-Azri, A.G. Dosado, M.A. Nadeem, D. Sun-Waterhouse, H. Idriss, and G.I.N. Waterhouse, "Effect of TiO_2 polymorph and alcohol sacrificial agent on the activity of Au/TiO_2 photocatalysts for H_2 production in alcohol–water mixtures," *J. Cat*., **329** 499–513 (2015). doi:10.1016/j.jcat.2015.06.014.
32) C.R. López, E.P. Melián, J.A. Ortega, D.E. Santiago, J.M. Doña, and O. González, "Comparative study of alcohols as sacrificial agents in H_2 production by heterogeneous photocatalysis using Pt/TiO_2 catalysts," *J. Photochem. Photobio.*, **312** 45–54 (2015). doi:10.1016/j.jphotochem.2015.07.005.